บทความวิจัย

การปรับปรุงประสิทธิภาพการเชื่อมและประสิทธิภาพเชิงกลในการใช้งานทางอุตสาหกรรม: การศึกษาโลหะเชื่อมโดยใช้วิธีเชื่อมแบบ GTAW

ยอดนภา เกษเมือง และ บัณฑิต อินทรีมีศักดิ์
สาขาวิชาวิศวกรรมการผลิตยานยนต์ คณะวิศวกรรมศาสตร์และเทคโนโลยี สถาบันการจัดการปัญญาภิวัฒน์
บัณฑิต วงศ์ทอง*
สาขาวิศวกรรมอุตสาหการ คณะวิศวกรรมศาสตร์ มหาวิทยาลัยธนบุรี

* ผู้นิพนธ์ประสานงาน โทรศัพท์ 08 1587 2173 อีเมล: Bundid.w@gmail.com
DOI: 10.14416/j.kmutnb.2026.11.005
รับเมื่อ 7 ธันวาคม 2568 แก้ไขเมื่อ 16 เมษายน 2569 ตอบรับเมื่อ 10 กรกฎาคม 2569 เผยแพร่ออนไลน์ 26 พฤศจิกายน 2569
© 2026 King Mongkut's University of Technology North Bangkok. All Rights Reserved.

บทคัดย่อ

งานวิจัยนี้ศึกษาการปรับปรุงกระบวนการเชื่อมด้วยอาร์คทังสเตนแก๊ส (GTAW) สำหรับรอยต่อโลหะต่างชนิดระหว่างท่อ A335 P11 และ A312 TP304 ซึ่งนิยมใช้ในงานอุตสาหกรรม เช่น หม้อไอน้ำแบบท่อน้ำ งานวิจัยนี้เน้นประสิทธิภาพของกระบวนการ การปรับปรุงคุณภาพ และการเพิ่มประสิทธิภาพเชิงกล โดยมุ่งเน้นที่ท่อที่มีเส้นผ่านศูนย์กลาง 89 มิลลิเมตร ความยาว 130 มิลลิเมตร และความหนา 5.54 มิลลิเมตร โดยใช้ลวดเชื่อม Ni625/ER NiCrMo-3 และปรับพารามิเตอร์การเชื่อมให้เหมาะสมด้วยเครื่องเชื่อม RILON TIG 200S กระแสเชื่อม 120 A ความเร็วในการเชื่อม 13.7 มิลลิเมตรต่อนาที และปริมาณการไหลของแก๊สปกคลุม 16 ลิตรต่อนาที ได้ทำการประเมินคุณสมบัติเชิงกลและโลหะวิทยา ซึ่งแสดงให้เห็นถึงความแข็งแรงดึงสูงสุด 675 เมกะปาสคาล และความแข็ง 230.4 HV การทดสอบแรงกระแทกเผยให้เห็นว่าบริเวณพื้นที่กระทบร้อน (HAZ) ของ A312 TP304 มีความเหนียวมากกว่า A335 P11 การทดสอบการดัดงอได้ยืนยันความสมบูรณ์ของโครงสร้างรอยเชื่อม โดยไม่พบรอยแตกที่การดัดงอ 180° ผลการค้นพบเหล่านี้เน้นย้ำถึงศักยภาพของ GTAW ในฐานะวิธีการเชื่อมโลหะต่างชนิดที่มีประสิทธิภาพและเชื่อถือได้ในกระบวนการผลิตทางอุตสาหกรรม ซึ่งจะช่วยเพิ่มประสิทธิภาพการผลิตและลดอัตราข้อบกพร่องในการใช้งานที่สำคัญ

คำสำคัญ: การใช้งานในอุตสาหกรรม การเพิ่มประสิทธิภาพต้นทุน คุณสมบัติเชิงกล ประสิทธิภาพการผลิต อาร์กทังสเตนแก๊ส

การอ้างอิงบทความ: ยอดนภา เกษเมือง, บัณฑิต อินทรีมีศักดิ์ และ บัณฑิต วงศ์ทอง, "การปรับปรุงประสิทธิภาพการเชื่อมและประสิทธิภาพเชิงกลในการใช้งานทางอุตสาหกรรม: การศึกษาโลหะเชื่อมโดยใช้วิธีเชื่อมแบบ GTAW," *วารสารวิชาการพระจอมเกล้าพระนครเหนือ*, ปีที่ 37, ฉบับที่ 1, หน้า 1–16, ม.ค.–มี.ค. 2570. เลขที่บทความ 271-098394, doi: 10.14416/j.kmutnb.2026.11.005.

Research Article

Improving Welding Efficiency and Mechanical Performance in Industrial Applications: A Study of Filler Metal Welds Using GTAW

Yodnapha Ketmuang and Bundit Inseemeesak

Automotive Manufacturing Engineering, Faculty of Engineering and Technology, Panyapiwat Institute of Management, Nonthaburi, Thailand

Bundit Wongthong*

Division of Industrial Engineering, Faculty of Engineering, Thonburi University, Bangkok, Thailand

* Corresponding Author, Tel. 08 1587 2173, E-mail: Bundid.w@gmail.com DOI: 10.14416/j.kmutnb.2026.11.005
Received 7 December 2025; Revised 16 Apirl 2026; Accepted 10 July 2026; Published online: 26 November 2026
© 2026 King Mongkut's University of Technology North Bangkok. All Rights Reserved.

Abstract

This research investigated the Gas Tungsten Arc Welding (GTAW) process for dissimilar metal joints between A335 P11 and A312 TP304 pipes, which are commonly used in industrial applications such as water-tube boilers. The study focused on improving process efficiency, weld quality, and mechanical performance using pipes with an outside diameter of 89 mm, a length of 130 mm, and a wall thickness of 5.54 mm. Welding was performed using Ni625/ER NiCrMo-3 filler metal and a RILON TIG 200S welding machine. The optimized welding parameters consisted of a welding current of 120 A, a welding speed of 13.7 mm/min, and a shielding gas flow rate of 16 L/min. Mechanical and metallurgical evaluations demonstrated a maximum tensile strength of 675 MPa and a hardness of 230.4 HV. The impact test revealed that the Heat-Affected Zone (HAZ) of A312 TP304 exhibited greater toughness than that of A335 P11. Bend tests confirmed the structural integrity of the welded joints, with no cracks observed after 180° bending. These findings highlight the potential of the GTAW process as an efficient and reliable method for dissimilar metal welding in industrial manufacturing, contributing to improved production efficiency and reduced defect rates in critical applications.

Keywords: Industrial Applications, Cost Optimization, Mechanical Properties, Manufacturing Efficiency, Gas Tungsten Arc

Please cite this article as: Y. Ketmuang, B. Inseemeesak, and B. Wongthong, " Improving welding efficiency and mechanical performance in industrial applications: A study of filler metal welds using gtaw," *The Journal of KMUTNB*, vol. 37, no. 1, pp. 1–16, Jan.–Mar. 2027 (in Thai), Art. no. 271-098394, doi: 10.14416/j.kmutnb.2026.11.005.

1. Introduction

A boiler is a closed vessel that utilizes heat generated from fuel combustion or electricity and passes it through water, converting the water into steam and increasing the pressure. This pressure is then transmitted to machinery in an industrial plant. Most boilers are manufactured primarily from carbon steel and constructed according to engineering principles and international standards. The steam produced is used in various industries, such as power generation, drying, and material processing. The size and complexity of boilers vary depending on the scope and requirements of the application [1].

The service life of the A335 P11 pipe is low at 1.5 years due to the high temperature and corrosion conditions inside the boiler. Therefore, an experiment was conducted to change to using A312 TP304 stainless steel pipe by welding the two types of metal together to extend the service life. The A312 TP304 pipe was expected to improve service life because of its higher corrosion and oxidation resistance to reduce creep strength and maintenance costs. This would also ameliorate the problem of power plant shutdowns, which increase power generation costs.

This study assessed the mechanical properties and metallurgical structure of Gas Tungsten Arc Welding (GTAW) to select the appropriate process for welding the two materials. Figure 1 shows a sample workpiece of dissimilar metals using the GTAW process, also known as Tungsten Inert Gas (TIG) welding. This welding process is easily controllable and cost-effective, making it ideal for precise welding of thin sheet metals, and it can be applied to a wide range of materials.

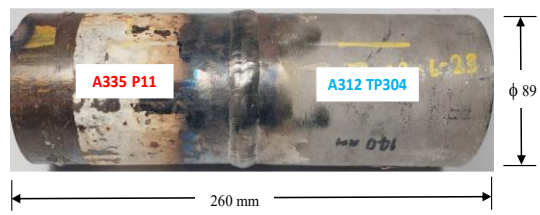


Figure 1 Speciments of A335 P11 and A312 TP304 pipes welded by the gas tungsten arc welding method.

Copious research studies have examined the metallurgical and mechanical properties of welding joints. Ramkumar *et al.* [2] investigated the microstructure and mechanical properties of dissimilar alloy welding of austenitic stainless steel (AISI 316L) and super duplex stainless steel (UNS S32750) by Continuous electric Current (CC) and Pulse electric Current (PC) by GTAW using ER2553 and ERNiCrMo-3 fillers. The tensile test results showed fractures of the AISI 316L base metal, while the bending test results showed that the ER2553 welds were cracked and torn due to large differences in the strength

of the AISI 316L base metal and the weld metal zone.

Chuaiphan and Srijaroenpramong [3] evaluated the metallurgical microstructure, mechanical properties, and corrosion resistance of dissimilar metal welding of 204Cu and 304 stainless steels by GTAW using 309L and 316L filler metals. Their results showed that the weld zones of both filler metals consisted of a delta ferrite phase and an austenite matrix phase. The delta ferrite phase in the 316L filler metal had a larger volume than the filler metal of 309L. The average hardness of the 309L welded metal was higher than 316L. Pitting corrosion resistance of the 309L filler metal was higher than 316L and also higher than the base metals 304 and 204Cu.

Tandon *et al.* [4] studied the metallurgical microstructure, mechanical properties, and corrosion resistance of dissimilar metal welding of austenitic stainless steel (316L) and low-Ni austenitic stainless steel (201) using the GTAW technique. The metallographic microstructural results revealed a balanced austenite/ ferrite content in the fusion zone for the two heat inputs. A low heat input process resulted in a faster cooling rate, which led to higher tensile strength and hardness test values. Similarly, the pitting corrosion resistance of the weld zone showed better properties in the low heat input process, with reduced dendrite length and smaller dendrite arm spacing. Ibrahim *et al.* [5] examined the mechanical properties in dissimilar butt joints between Ni medium manganese and nickel- chromium austenitic stainless steels processed by GTAW. Their results showed that the microstructure consisted of an austenite and delta ferrite matrix obtained by welding dissimilar butt joints. The weld had a low tensile strength at 610 MPa, which was lower than the Base Metals (BM) M-Mn SS, and Ni-Cr SS because of the uneven dendritic structure of the weld zone where Cr-carbide precipitation occurred.

Tandon *et al.* [6] used the GTAW method to join 201 and 316L austenitic stainless steels using different filler metals (316L, 309L, and 309LMo). In the weld zone, the microstructures contained varying amounts of ferrite. In the filler metals E316L, E309L, and E309LMo, the ferrite amounts were 8.78, 9.05, and 12.69 units, respectively. All the welds exhibited ductile fracture characteristics. Zisopol *et al.* [7] performed degradation tests on the hardness and tensile strength of Shore A butt-welded PE100 SDR11 pipes used for natural gas transportation. The results showed that the tensile strength increased when increasing the curing time by 6.5% for the 10-year cured samples and 6.16% for the 20-year cured samples.

For the unwelded samples, the tensile strength decreased by 3.57% for the 10-year and increased by 5.84% for the 20-year cured samples. Artificial aging of the natural gas transmission and distribution pipeline for 10 and 20 years did not significantly affect the Shore A hardness.

However, the previous research lacked comprehensive mechanical testing that met petrochemical standards. This study investigates the effects of GTAW using Ni625/ER NiCrMo-3 filler metal on A335 P11 and A312 TP304 pipes. Macro and microstructural analyses were conducted, together with tensile, hardness, bending, and impact tests. Alloying elements in the weld zone were also examined using the Energy Dispersive Spectroscopy (EDS) technique.

2. Materials and Methods

2.1 Welding Procedure

The pipes were 5.54 mm thick, 130 mm long, with 89 mm Outside Diameter (OD). The first pipe metal was ASTM A335 P11 steel with the chemical composition [8] shown in Table 1. The second pipe metal was A312 TP304 stainless steel with the chemical composition [9] shown in Table 2. The filler metal used was Ni 625/ER NiCrMo-3 with a diameter of 2.4 mm. The chemical composition [10] of the filler metal is shown in Table 3. The GTAW process was conducted according to AWS D1.1 standards [11].

Table 1 Chemical composition of ASTM A335 P11 (%wt).

Material	A335 P11
C	0.05 – 0.15
Mn	0.30 – 0.60
P	≤ 0.025
S	≤ 0.025
Si	0.50 – 1.00
Cr	1.00 – 1.50
Mo	0.44 – 0.65

Table 2 Chemical composition of ASTM A312 TP304 (%wt).

Material	A312 TP304
C	≤ 0.080
Mn	≤ 2.00
P	≤ 0.045
S	≤ 0.030
Si	≤ 1.00
Cr	18.0 – 20.0
Ni	8.0 – 11.0

Table 3 Chemical composition of Ni 625/ER-NiCrMo-3 (%wt).

Filler metal	AWS A5.18 ER 70S-6
C	0.02
Si	0.20
Mn	0.03
P	0.006
S	0.001
Cr	22.0
Ni	64.0
Mo	9.00
Nb + Ta	3.60

The process began by cutting and preparing the pipes. The joint was formed by machining a notch with a total groove angle of 60°. The welding sequence for each bead is illustrated in Figure 2.

Argon is used as the shielding gas in the GTAW process. Its flow rate is regulated by a flow meter mounted on the torch head, allowing accurate control during welding, and the welding speed is manually controlled by the welder. In this study, a welding speed of 13.7 mm/min was applied. The welding speed is closely linked to welding current, with a higher current enabling faster travel speed. This relationship influences production quality and the overall heat input to the weld bead. The heat input significantly affects the weld characteristics and the properties of the HAZ, including hardness and tensile strength. In GTAW with argon shielding, only 60% of the generated heat is effectively utilized in the weld bead. The remaining heat is dissipated through the shielding gas, radiation, and other losses. The welding parameters are summarized in Table 4. All the welding was performed in the 1G position, which refers to the flat position used for groove welds. In this setup, the workpiece lies horizontally while the welder works from above. Gravity assists the molten metal in flowing into the joint, making the weld pool easier to manage and resulting in a smoother, more consistent bead.

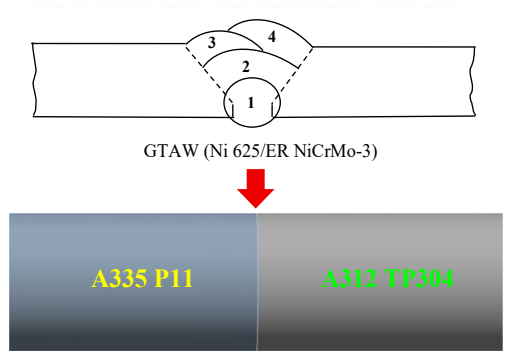


Figure 2 Standard requirements for joints and welding procedure.

Table 4 Welding parameters for the GTAW.

Parameter	Unit
Electrode diameter	2.4 mm
Arc voltage	120 V
Current intensity	95 A
Welding speed	13.7 mm/min
Shielding gas flow volume	16 L/min

2.2 Metallography

In this research, the metallographic structure examination was performed using an Olympus laser microscope OLS 4000, which captured the details of the workpiece in 3D at high resolution. The microstructure was examined at five points, as shown in Figure 3, as the base metal1 (BM1, P11), the heat affected zone1 (HAZ1), the weld metal zone, the heat affected zone2 (HAZ2) and the base metal2 (BM2, 304). The EDS technique, using a Scanning Electron Microscope (SEM) model

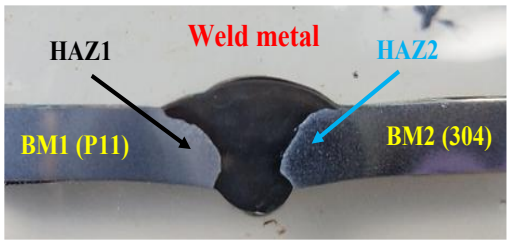


Figure 3 Locations of the five points used for metallurgical structure inspection.

JEOL: JSM- 7800F Prime, was used to analyze the chemical composition of the elements at the weld metal zone.

2.3 Mechanical Properties Test

The tensile test was carried out using a SHIMADZU: EHF-EV100K1-070-0A universal tensile machine of 300 KN capacity. The parameter values were input directly from the monitor in the form of numbers and graphs. This test determines the tensile strength, the yield strength, and the percentage of elongation of the weld. The parameter values were set according to the ASTM E8 2014 standard, as shown in Figure 4. The standard gauge length of the welded specimen was 25 mm, keeping the weld interface at its center.

The hardness test was performed using a Vickers hardness tester (Anton Paar MHT-10). The hardness values were measured at various areas of the weld, including the BM, the HAZ, and the Weld Metal (WM), as illustrated in Figure 5, with a load of 10 kgf and a holding time of 10 seconds. The pyramid-shaped diamond indenter produced a square indentation. The hardness tests were performed along two lines, with the first line testing the hardness at the top of the weld and the second line testing the hardness at the bottom of the weld [9]. There were 10 test points per line, applying a force of 10 kg and holding time of 10 seconds. The test was conducted according to ASTM E3-11.

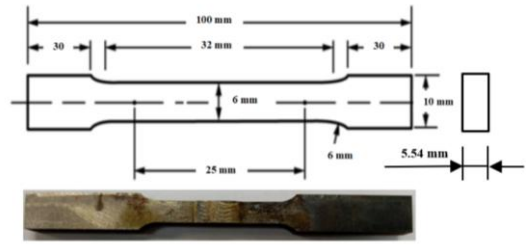


Figure 4 Preparation of the tensile test specimen according to ASTM E8 2014.

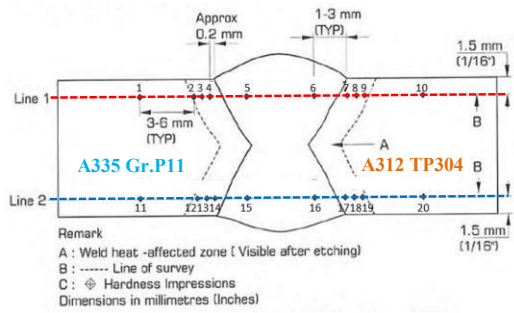


Figure 5 Location of the hardness test 2 lines, 10 points each line.

The bending tests, following ASME E90-21 (Figure 6), were conducted on welds produced using the GTAW process. Four specimens were pre-ground to remove excess weld metal before

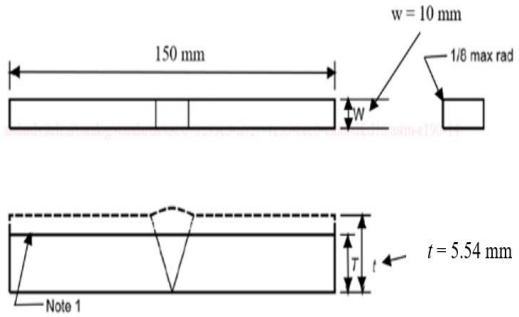


Figure 6 Dimensions of the bending test specimen according to ASTM E90-21.

testing. The bending tests included face bend and root bend.

The Charpy impact test was performed by striking the test piece once with a swing to break it under specified conditions. The test piece must be notched with the size and characteristics specified in ASTM A370-21. The test piece had a V-notch in the center, with three pieces per test point obtained from the weld metal, the HAZ (P11) and the HAZ (TP304) as specified in ASTM A370-21 (Figure 7). The test piece was placed on two supports 40 mm apart, and each end of the specimen was firmly clamped. The notches were arranged in the center, opposite to the direction of the hammer swing. This type of clamping of the test piece is convenient fast, and suitable for testing specimens at high and low temperatures. The hammer swing in a V-shaped, 30 degrees angle, with the radius of curvature at the sharp end 2–2.5 mm.

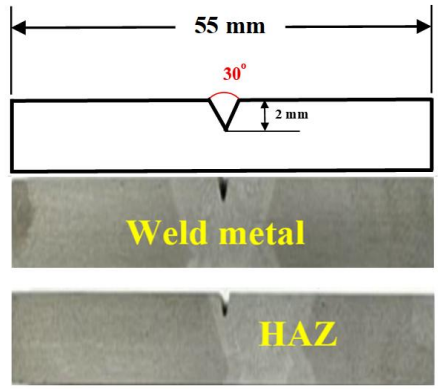


Figure 7 Preparation of welded pieces for impact Testing.

3. Results and Discussions

3.1 Metallography

The results of the microstructural examination at the five points are as follows: Figure 8 shows the base metal area of A335 P11 steel (BM1) at a magnification of 500x, 50 µm. The microstructure of the P11 steel pipe consisted of ferrite and pearlite, with small amounts of bainite and carbides [12]. Figure 9 presents an image of HAZ1 of the P11 steel pipe at a magnification of 500x, 50 µm. The microstructure consisted of pearlite, ferrite, granular bainite, and some granular carbides. Coarse ferrites were distributed along the grain boundaries in a lattice pattern, with small amounts of carbides [13]. The chemical composition, analyzed using the EDS technique, revealed chromium as the highest component. Details of the other elements are shown in Figure 10.

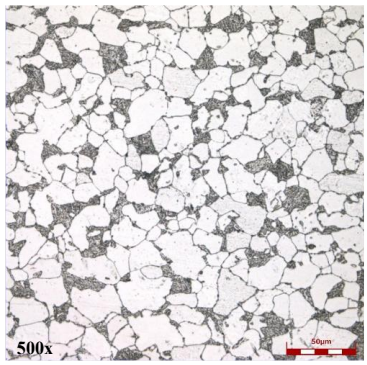


Figure 8 Microstructure of the base metal area of A335 P11 steel (Base metal: BM1).

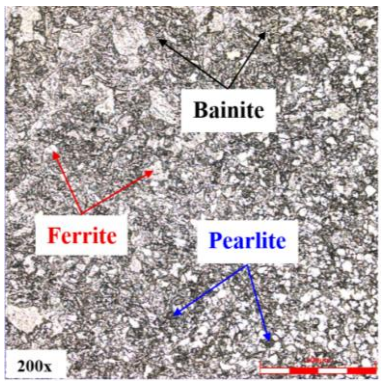


Figure 9 Microstructure in the heat affected zone (HAZ1).

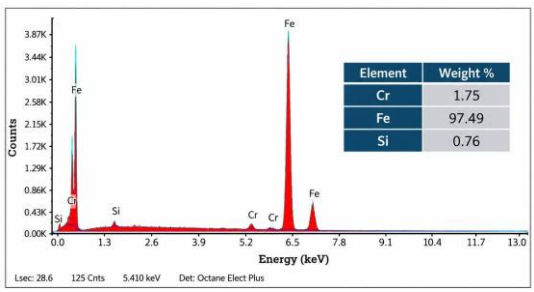


Figure 10 EDS results on the heat affected zone (HAZ1).

In Figure 11, the microstructure of the weld metal at 100x, 400 μm, consisted of a ferrite dendrite and austenite matrix [14]–[15], Ferrite dendrites prevent crack expansion along the grain boundaries, reducing crack propagation along the solidification structure and decreasing the likelihood of cracking. An austenitic Face-Centered Cubic (FCC) structure facilitates dislocation but prevents brittleness; the welds are ductile, enhancing corrosion resistance. The chemical compositions of the welds were examined using the EDS technique. Results revealed that most elements were components of the welding wire, with nickel having the highest content. Details of the other elements are shown in Figure 12.

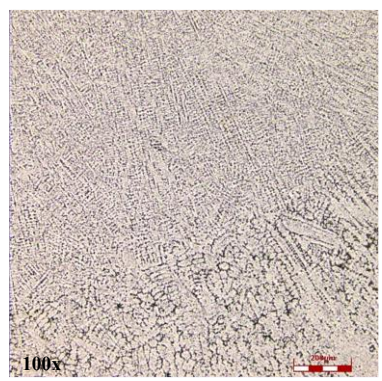


Figure 11 Microstructure in the weld metal zone.

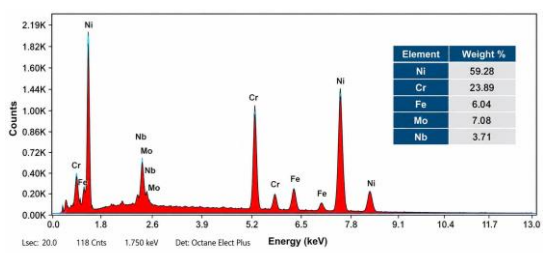


Figure 12 EDS analysis of the weld metal.

Figure 13 shows the HAZ2 images at a magnification of 200x, 200 µm. The microstructure of both weld metals consisted of solidified delta ferrite with skeletal morphology. The ferrite formed at the austenite grain boundaries. A comparison of the microstructural images with the findings indicated significant similarities. Baskutis *et al*. [16] investigated dissimilar welds between stainless and structural steels also reported the formation of comparable austenitic grains and dendritic structures to those observed in this investigation. Furthermore, the weld metal exhibited a microstructural transformation from cellular to columnar dendrites, a transition consistent with established solidification theories regarding variations in cooling rates and the degree of undercooling during the welding process. The chemical composition, analyzed using the EDS technique, revealed chromium as the highest component. Details of the other elements are shown in Figure 14.

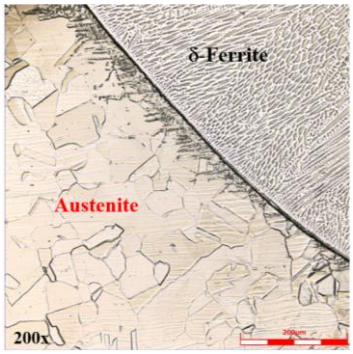


Figure 13 Microstructure in the heat affected zone (HAZ2).

Figure 15 presents an image of the base metal area of A312 TP304 stainless steel (BM2) at 500x, 50 µm. The microstructure revealed a twin-phase austenitic stainless steel.

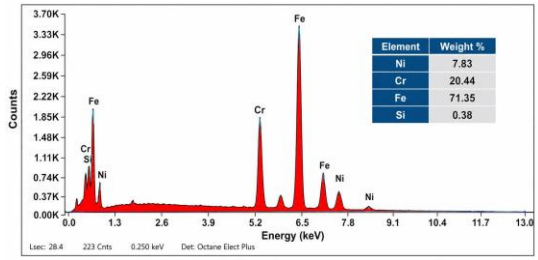


Figure 14 EDS results on the heat affected zone (HAZ2).

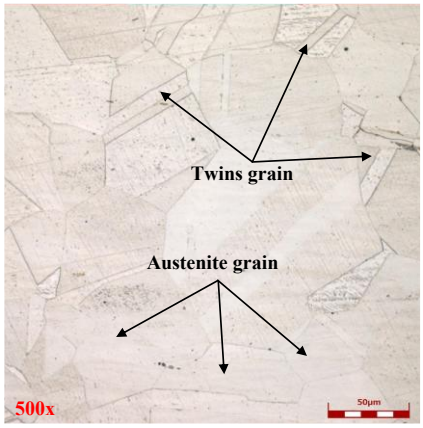


Figure 15 Microstructure in the base metal (BM2).

3.2 Tensile Test

The tensile test results from the stress-strain curves of the welded specimens in Figure 16 showed that all stresses had similar fracture values. All the fractures occurred in the base metal A335 Gr. P11, particularly in the HAZ as shown in Figure 17 and Table 5. Therefore, the weakest part of the joint was the base metal

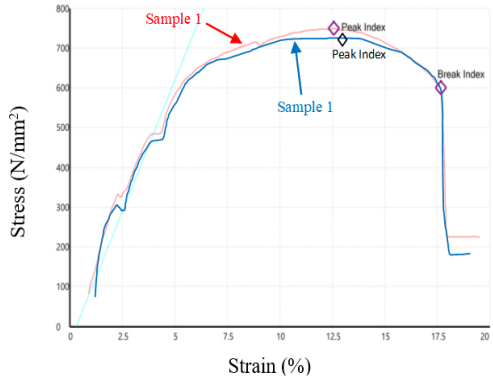


Figure 16 Stress-strain curves of specimen 1 and 2 of welding A312 TP304 and A335 P11.



Figure 17 Photograph of the tensile specimens showing the location of fracture in the weld metal.

Table 5 The results of welded tensile test.

No.	Yield strength (MPa)	UTS (MPa)	Elongation %	Location of fracture
1	325	670	10.14	Out of Weld (A335 Gr.P11)
2	330	681	10.62	Out of Weld (A335 Gr.P11)

A335 Gr. P11. The yield strength determined experimentally in this study was 330 MPa, which is consistent with previous findings [17] regarding the mechanical performance of dissimilar joints processed by GTAW. Li *et al.* [17] demonstrated that the mechanical integrity of dissimilar butt joints is highly dependent on the specific microstructure formed during welding. Furthermore, the fracture location observed in the Heat-Affected Zone (HAZ) of ASTM A335 steel aligns with typical failure patterns in dissimilar welds where the HAZ becomes the weakest region due to thermal cycling, as also discussed in recent studies on austenitic joint performance. The microstructural changes in the HAZ of P11 are mainly attributed to grain coarsening and martensitic transformations during thermal cycling, which promote further grain growth [17].

3.3 Hardness Measurement

The results of the hardness test after the GTAW process are shown in Figure 18. The hardness profile of the weld was divided into 5 zones as BM P11, HAZ P11, WM, HAZ TP304, and BM TP304. The hardness in each area for all 10 points along line 1 (red line) was highest at point 4, the HAZ P11 at 230.4 HV, and the lowest value was at point 1 (153.8 HV).The HAZ P11 from test points 2–4 had a higher hardness value than the WM at points 5–6, but a higher hardness value than the HAZ TP304 at points 7–9. The hardness value in each area of all 10 points along line 2 (blue line), was highest at point 4, HAZ P11 at 209.3 HV, and lowest at point 1 (154.9 HV).The HAZ P11 from test points 2–4 had a higher hardness value than the WM at

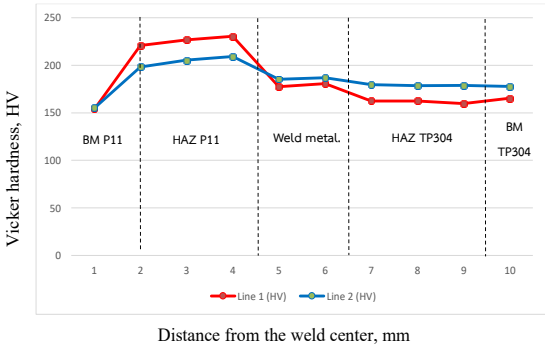


Figure 18 Hardness profiles of both sides of the weld metals.

points 5–6, but the hardness value was higher than the HAZ TP304, at points 7–9.

The heat generated during welding changes the microstructure of the weld metal, leading to solidification and an increase in hardness. The HAZ near the BM had a higher hardness value than the WM, but lower than the BM. This trend was consistent across both compression test paths. The maximum hardness was observed in the HAZ of P11 steel due to the formation of martensitic or bainitic phases as a result of rapid cooling, with grain refinement and carbide precipitation [17].

3.4 Bending Test

The bending of the four specimens was tested at 25°C (room temperature) and 50% relative humidity when bent at 180°, as shown in Table 6. Figure 19 presents the corresponding macrostructures of the four specimens after testing. The face bending test in Figure 19(a), only surface bulging was observed, with no visible cracks or fractures. The root bending test results are displayed in Figure 19(b). After all the bending tests, the filled joints exhibited no cracks, fractures, tears, or any other defects. Different types of bending tests were applied, with each yielding consistent results showing no

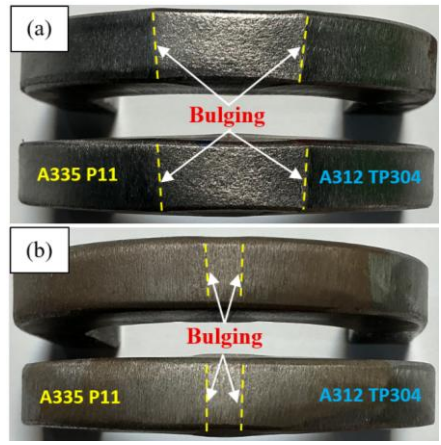


Figure 19 Macrostructures of the four specimens: (a) bulging after the face bend test, and (b) bulging after the root bend test.

Table 6 Bend testing of the weld joints.

No.	Type of Bend	Mandrel Diameter (mm)	Bend Angle (degree)	Visually examined result for surface discontinuity
1	Face bend	22	180°	No Surface Discontinuity
2		22	180°	No Surface Discontinuity
3	Root bend	22	180°	No Surface Discontinuity
4		22	180°	No Surface Discontinuity

discontinuities. When compared with previous research [18], the results show similar characteristics of high joint integrity and ductility. Prasetia *et al*. [18] investigated dissimilar stainless steel welds confirmed that using appropriate GTAW techniques produces defect-free joints capable of withstanding significant plastic deformation without cracking, which supports the findings of this study regarding surface bulging without fractures. This result demonstrated that the welding procedures used to produce the specimens were performed with high quality and reliability [18]. The welds demonstrated excellent ductility and structural integrity, even in dissimilar metal combinations. Their capacity to withstand bending deformation without failure was attributed to the austenitic structure within the weld zone. This generated a highly ductile microstructure that effectively accommodated plastic deformation. This behavior was linked to the use of filler materials specifically intended for dissimilar metal welding, which reduces the mechanical property mismatch between low-alloy steel (P11) and stainless steel (TP304). Consequently, proper melting and mixing of the base metals produced a defect-free joint without porosity or weak areas.

3.5 Charpy Impact Test

The impact specimens were tested at 25°C (room temperature). The absorbed energy as a function of test conditions, with the post-impact fracture characteristics are presented in Figure 20, with detailed results listed in Table 7.

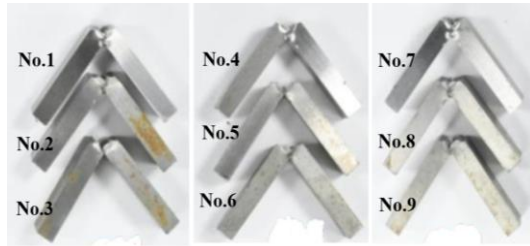


Figure 20 Characteristics of specimens after impact testing.

Table 7 The results of welded Impact test.

No.	Location of Charpy V-Notch	Absorbed energy (J)	
		Individual	Average
1	Weld metal	44.7	48.73
2		46.6	
3		54.9	
4	HAZ	32.7	64.47
5	(A335 Gr.P11)	89.6	
6		71.1	
7	HAZ	89.2	87.53
8	(A312 TP304)	86.5	
9		86.9	

The highest average absorbed energy was recorded in the HAZ of TP304 at 87.53 J, followed by the HAZ of P11 at 64.47 J. The WM showed the lowest average absorbed energy of 48.73 J. The results indicated that the HAZ of TP304 had superior toughness compared to both the HAZ of P11 and the WM [19]. This variation was explained by the inherently high

toughness of austenitic stainless steel (TP304), which is associated with its face-centered cubic crystal structure that promotes greater plastic deformation. By contrast, the weld metal contained δ – ferrite and dendritic microstructures, which can adversely affect impact toughness and lead to reduced energy absorption.

4. Conclusion

The reasons for the dissimilar welding results between P11 and TP304 steel using GTAW are summarized below.

The weld metal had a dendritic ferrite structure within an austenite matrix. The EDS results indicated that the composition was mainly from the filler metal, with Ni as the highest element (59.28%), followed by Cr (23.89%).

The tensile tests showed that all fractures occurred in the P11 base metal, especially in the HAZ. Hardness results indicated the highest values in the P11 HAZ and the lowest in the P11 (BM), matching the observed fracture locations. By contrast, the TP304 HAZ showed higher impact toughness due to its austenitic microstructure, which enhanced energy absorption and fracture resistance.

The impact test results showed that the HAZ of TP304 had the highest average absorbed energy of 87.53 J, followed by the HAZ of P11 (64.47 J), while the WM had the lowest at 48.73 J. Overall, the HAZ of TP304 exhibited the optimal toughness.

Welding experiments were conducted on two materials to extend boiler tube service life under high-temperature and corrosive conditions. The results suggested reduced maintenance costs, with fewer costly power plant shutdowns.

5. Acknowledgement

This research was supported by the Automotive Manufacturing Engineering Department, Faculty of Engineering and Technology, Panyapiwat Institute of Management of Technology for research equipment and facilities. The authors express their gratitude to the National Metal and Materials Technology Center (MTEC) for providing assistance and guidance during the experiments.

References

[1] Koch Applied Solutions. (2025 , Jan.) . Boilers 101. [Online]. Available: https://www.kochapplied.com/blog/boilers-101/

[2] K. D. Ramkumar, A. Singh, S. Raghuvanshi, A. Bajpai, T. Solanki, M. Arivarasu, N. Arivazhagan, and S. Narayanan, “Metallurgical and mechanical characterization of dissimilar welds of austenitic stainless steel and super-duplex stainless steel–A comparative study,” *Journal of Manufacturing Processes*, vol. 19, pp. 212–232, 2015, doi: 10.1016/j.

jmapro.2015.04.005.

[3] W. Chuaiphan and L. Srijaroenpramong, "Evaluation of microstructure, mechanical properties and pitting corrosion in dissimilar of alternative low-cost stainless-steel grade 204 Cu and 304 by GTA welding joint," *Journal of Materials Research and Technology,* vol. 9, no. 3, pp. 5174–5183, 2020, doi: 10.1016/j.jmrt.2020.03.034.

[4] V. Tandon, M. A. Thombre, A. P. Patil, R. V. Taiwade, and H. Vashishtha, "Effect of heat input on the microstructural, mechanical, and corrosion properties of dissimilar weldment of conventional austenitic stainless steel and low-nickel stainless steel," *Metallography, Microstructure, and Analysis*, vol. 9, pp. 668–677, 2020, doi: 10.1007/s13632-020-00681-y.

[5] I. R. Ibrahim, M. Khedr, T. S. Mahmoud, H. A. Abdel-Aleem, and A. Hamada, "Study on the mechanical performance of dissimilar butt joints between low Ni Medium-Mn and Ni-Cr austenitic stainless steels processed by gas tungsten arc welding," *Metals*, vol. 11, 2021, Art. no. 1439, doi: 10.3390/met11091439.

[6] V. Tandon, A. P. Patil, and S. Kowshik, "Impact of filler electrodes on welding properties of dissimilar welded 316L/201 austenitic stainless steels," *Engineering proceedings*, vol. 59, 2023, Art. no. 90, doi: 10.3390/engproc2023059090.

[7] D. G. Zisopol, M. Minescu, and D. V. Iacob, "A study on the influence of aging of the butt-welded PE100 SDR11 on shore a hardness and tensile strength," *Engineering, Technology & Applied Science Research,* vol. 14, no. 1, pp. 12722–12727, 2024, doi: 10.48084/etasr.6635.

[8] ASTM A335. P11 Pipe Specification (Chrome Moly Seamless Pipe). Octal Steel. [Online]. Available: https://www.octalsteel.com/resources/astm-a335-p11-pipe/

[9] ASTM A312. Stainless Steel Pipe. Octal Steel. [Online]. Available: https://www.octalsteel.com/resources/astm-a312-tp304-tp316-ss-pipe/

[10] SMT-625. AWS A5.14/ ASME SFA5.14 ERNiCrMo-3. [Online]. Available: https://arcweldingservice.com/content/file/product/0618201592461732.pdf

[11] AWS D1.1:2000. Structural Welding Code-Steel. American Welding Society. [Online]. Available: https://law.resource.org/pub/us/cfr/ibr/003/aws.d1.1.2000.pdf

[12] R. Chaudhari and A. Ingle, "Experimental investigation of dissimilar metal weld of SA335 P11 and SA312 TP304 formed by Gas Tungsten Arc Welding (GTAW)," *Transactions of the Indian Institute of Metals*, vol. 72,

pp. 1145–1152, 2019, doi: 10.1007/s12666-019-01587-2.

[13] M. Ahmadi and S. E. Mirsalehi, "Investigation on microstructure, mechanical properties and corrosion behavior of AISI 316L stainless steel to ASTM A335-P11 low alloy steel dissimilar welding joints," *Materials at High Temperatures,* vol. 32, no. 6, pp. 627–635, 2015, doi: 10.1179/1878641315Y.0000000009.

[14] R. Chaudhari and A. Ingle, " An empirical research on dissimilar metal weld of SA335 P11and SA312 TP304 formed by Metal Inert Gas (MIG) welding," *International Journal of Recent Technology and Engineering (IJRTE)*, vol. 8, no.2, pp. 5008–5012, 2019, doi: 10.35940/ijrte.B1079.078219.

[15] H. Wanga, K. Wanga, W. Wanga, L. Huanga, P. Penga, and H. Yu, " Microstructure and mechanical properties of dissimilar friction stir welded type 304 austenitic stainless steel to Q235 low carbon steel," *Materials Characterization*, vol. 155, 2019, Art. no. 109803, doi: 10.1016/j.matchar.20 19.109803.

[16] S. Baskutis, J. Baskutiene, R. Bendikiene, A. Ciuplys, and K. Dutkus, " Comparative research of microstructure and mechanical properties of stainless and structural steel dissimilar welds," *Materials*, vol. 14, 2021, Art. no. 6180, doi.org/10.3390/ma14206180.

[17] C. Li, G. Qin, Y. Tang, B. Zhang, S. Lin, and P. Geng, " Microstructures and mechanical properties of stainless-steel clad plate joint with diverse filler metals," *Journal of Materials Research and Technology,* vol. 9, no. 2, pp. 2522– 2534, 2020, doi: 10. 1016/j.jmrt.2019.12.083.

[18] T. G. Prasetia, M. Ariyon, F. Fitriani, A. Sebayang, and E. Tarigan, " Comparative analysis of compressive strength of steel tubing pipe welding results using smaw and mig welding with 140A current," *International Journal of Engineering, Science and Information Technology*, vol. 5, no. 1, pp. 136–139, 2025, doi: 10. 52088/ijesty.v5i1.644.

[19] S. Sirohi, S. M. Pandey, A. Swierczynska, G. Rogalski, N. Kumar, M. Landowski, D. Fydrych, and C. Pandey, " Microstructure and mechanical properties of Combined GTAW and SMAW dissimilar welded joints between inconel 718 and 304L austenitic stainless steel," *metals*, vol. 13, pp. 14, 2023, doi: 10.3390/met13010014.